Biophysical Chemistry 195 (2014) 1–7

Contents lists available at ScienceDirect

Biophysical Chemistry

journal homepage: http://www.elsevier.com/locate/biophyschem

Structural stability of *E. coli* trigger factor studied by synchrotron small-angle X-ray scattering

Yi Shi [a,*], Masaji Shinjo [b], Jun-Mei Zhou [c], Hiroshi Kihara [b,**]

[a] Shanghai Advanced Research Institute, Chinese Academy of Sciences, 99 Haike Road, Zhangjiang Hi-Tech Park, Pudong, Shanghai 201210, China
[b] Department of Physics, Kansai Medical University, 2-5-1, Shin-Machi, Hirakata 573-1010, Japan
[c] National Laboratory of Biomacromolecules, Institute of Biophysics, Chinese Academy of Sciences, 15 Datun Road, Beijing 100101, China

HIGHLIGHTS

- We used SAXS to study structural characteristics and unfolding transitions of TF.
- C-terminal region plays an important role in the structural stabilities of TF.
- N-domain of TF is relative structural independent.

GRAPHICAL ABSTRACT

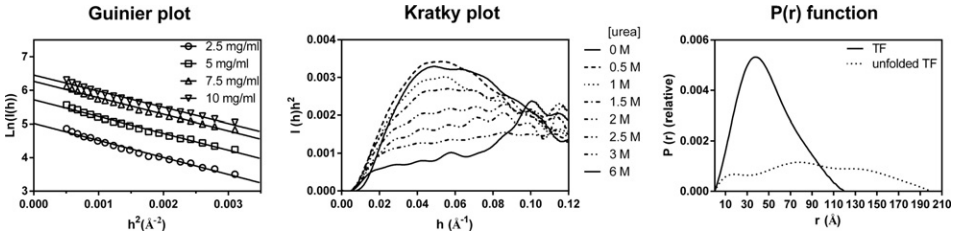

ARTICLE INFO

Article history:
Received 22 May 2014
Received in revised form 16 July 2014
Accepted 16 July 2014
Available online 26 July 2014

Keywords:
C-terminal truncation
Folding
Stability
Small-angle X-ray scattering
Trigger factor

ABSTRACT

Solution small-angle X-ray scattering (SAXS) is an effective technique for quantitatively measuring the compactness and shape of proteins. We use SAXS to study the structural characteristics and unfolding transitions induced by urea for full length *Escherichia coli* trigger factor (TF) and a series of truncation mutants, obtaining and comparing the radiuses of gyration (R_g), the distance-distribution function ($P(r)$ function) and integrated intensity of TF variants in native and unfolding states. The C-terminal 72-residue truncated mutant TF360 exhibited dramatic structural differences and reduced stability compared with the whole TF molecule, while the N-domain truncated mutant MC maintained its compact structure with reduced stability. These results indicate that the C-terminal region of TF plays an important role in the structural and conformational stabilities of the TF molecule, while the N-domain is relatively independent.

1. Introduction

Nascent polypeptides must fold into correct three-dimensional structures to perform their biological function. Protein folding is often hampered by protein aggregation, which can be prevented by a network of chaperones in the cell [1–4]. Trigger factor (TF) is a eubacterial chaperone that associates with ribosomes at the nascent peptide-exit tunnel and occurs in excess free in the cytosol, therefore it is the first chaperone to bind newly synthesized polypeptides and assist their folding before passing them to downstream chaperone systems [5–19]. Due to its position at the ribosome exit tunnel, TF also plays an important role in the regulation of protein translocation.

Escherichia coli TF is 432 residue long and composed of an N-terminal ribosome-binding tail (N-domain, 1–144), a middle domain with peptidyl-prolyl cis/trans isomerase (PPIase) activity (M-domain, 145–247) and a C-terminal domain (C-domain, 248–432) that is involved in chaperone activity [18,20,21].

Recently, a number of trigger-factor structures that clarify the structure of TF have been determined. These include the ribosome-binding

* Correspondence to: Y. Shi, Shanghai Advanced Research Institute, Chinese Academy of Sciences, 99 Haike Road, Zhangjiang Hi-Tech Park, Pudong, Shanghai, 201210, China. Tel.: +86 21 20325175; fax: +86 21 20325064.
** Correspondence to: H. Kihara, Department of Physics, Kansai Medical University, 2-5-1, Shin-Machi, Hirakata 573-1010, Japan.
E-mail addresses: shiy@sari.ac.cn (Y. Shi), kiharah1234@gmail.com (H. Kihara).

http://dx.doi.org/10.1016/j.bpc.2014.07.002
0301-4622/

domain of *E. coli* TF [22], full-length *E. coli* TF [23], a C-terminally truncated *Vibrio cholerae* TF [24], a ribosome-bound *Deinococcus radiodurans* TF N-terminal domain [25,26], a *Mycoplasma genitalium* TF PPIase domain [27] and *Thermotoga maritima* TFN-terminal and C-terminal domain [28].

Studies of the structure of TF-ribosome [23,25,26] and TF-S7 [29] complexes have provided a detail on the interactions between TF and the ribosome and those between TF and the substrate. These studies have also identified associations that can describe the proposed monomeric and dimeric species [22,24].

Solution small-angle X-ray scattering (SAXS) is a powerful tool that provides structural information on the shape and size of macromolecules in solution [30,31]. Scattering intensity from a dilute monodisperse solution of macromolecules is proportional to the spherically averaged single-particle scattering, scattering intensity at various scattering angles can be collected and the shape and size of macromolecules can be calculated from the scattering intensity [30–32]. Therefore SAXS in solution can yield low-resolution information only (from 1 to 100 nm) but are applicable in a broad range of conditions and particle sizes [32]. SAXS permits analysis of biological macromolecules and their complexes under close to physiological conditions, and is particularly useful when high-resolution structural information, such as that from x-ray crystallography or NMR, is not yet available [32]. Although SAXS doesn't inform directly on secondary structure such as circular dichroism (CD) and nuclear magnetic resonance (NMR), but it is sensitive to overall conformational changes such as changes in the shape/morphology of the protein, expansion of the protein [30,31]. Studies have taken advantage of the SAXS method to analyze the three-dimensional structures of proteins and monitor their conformational changes under various conditions [33–36].

N- and C-domains of TF synergistically perform the chaperone function in vitro and in vivo, but how the domain affects the structural stability of the intact molecule is not clear. Here, we use SAXS to study the role of various truncations on the structural stability of TF.

2. Materials and methods

2.1. Reagents

Urea was purchased from Sigma. All other chemicals were local products of analytical grade.

2.2. Generation of TF variants

A number of truncation mutants of the TF were constructed, namely: TF419, TF360 and MC, in which the C-terminal 13, 72 or the entire N-domain were deleted, respectively. Proteins were purified according to the method of Zeng et al. [37]. The molecular masses of TF, TF419, TF360 and MC were 48.2, 46.6, 39.9 and 32.4 kD, respectively. The absorbance coefficients of ε_{280nm} = 15,930, 17,159, 13,823 and 9978 M^{-1} cm^{-1} were used to determine the protein concentrations of TF, TF419, TF360 and MC, respectively [37].

2.3. Synchrotron SAXS measurements

X-ray solution-scattering measurements were performed at the beam line 15A small angle installation (BL-15A) of Photon Factory of High Energy Accelerator Research Organization (KEK), Tsukuba, Japan. A bent-crystal, horizontally-focusing monochromator and a vertically focusing mirror provided a stable beam of photons, with a wavelength of 1.5 Å. The camera length (i.e., the sample-to-detector distance) was 1639 mm in the first experiment and 1744 mm in the second. We measured proteins (5 mg/ml) in a 0.1 M, pH 7.5 PBS buffer containing different concentrations of urea (0, 0.5, 1, 1.5, 2, 2.5, 3 and 6 M). The background data for the buffer solution with different concentrations of urea was collected before data collection for the protein solutions [34,38].

2.4. SAXS data process

The correction of the SAXS data for the difference in electron density between the protein and solvent molecules, as well as for X-ray absorption by the solution, was made according to known standard procedures [30]. The radius of gyration, R_g, was estimated by Guinier approximation,

$$\mathrm{I}(h) = \mathrm{I}(0)\exp\left(-\frac{R_g^2 h^2}{3}\right) \tag{1}$$

where h is the scattering vector given by $h = (4\pi\sin\theta)/\lambda$ (2θ is the scattering angle and λ is the wavelength of X-rays) and $\mathrm{I}(0)$ is the scattering intensity at zero angle [30,31]. For the native globular protein, the R_g was calculated by fitting the curve $\mathrm{Ln}\mathrm{I}(h)$ against h to the Guinier equation in the region between 0.0005–0.0035 $Å^{-2}$ in h. For denatured states, the Guinier approximation cannot be used because the previous approximation is valid only for $R_g{}^*h \le 1$ [34]. In this case, the scattering profile can be described to a first approximation in the small h region ($R_g{}^*h \le 3$) by the Debye function,

$$\mathrm{I}(h)/\mathrm{I}(0) = \left(2/x^2\right)\left(x-1+e^{-x}\right) \tag{2}$$

Where $x = h^{2*}R_g{}^2$ [34]. The globularity of the protein molecule was examined using a Kratky plot, i.e., $K = \mathrm{I}(h)h^2$ versus h [39,40]. The distance-distribution function, $P(r)$, was calculated using the GNOM program [41].

2.5. Analysis of equilibrium data

Equilibrium data were fitted to a two-state model using the following equations:

$$Y = f_N Y_N + f_U Y_U \tag{3}$$

$$f_N + f_U = 1 \tag{4}$$

$$f_N = \frac{[N]}{[N]+[U]} \tag{5}$$

$$K = \frac{[U]}{[N]} \tag{6}$$

$$\Delta G = \mathrm{RTlnK} = \Delta G^0 - m_G[\mathrm{urea}] \tag{7}$$

so,

$$K = \exp\left(\frac{m_G[\mathrm{urea}]-\Delta G^0}{RT}\right) \tag{8}$$

or

$$K = \exp\left(\frac{m_G([\mathrm{urea}]-C_m)}{RT}\right) \tag{9}$$

where Y is the experimentally-measured signal (refers to $\mathrm{I}(h)h^2$ intensity at peak of Kratky plot or integrated intensity in this study) at a given denaturant concentration [urea]; Y_N and Y_U are the signals of TF for the native and unfolded states, respectively; f_N and f_U are the fraction of the

native and unfolded states, respectively; K is the apparent equilibrium constant; ΔG is the free-energy change upon unfolding; ΔG^0 is the free-energy change upon unfolding in the absence of denaturants; m_G is the linear dependence of ΔG upon the denaturant concentration; C_m represents the denaturant concentration at which 50% of the molecules are folded; R is the gas constant; and T is the absolute temperature [42,43]. The program GraphPad Prism 5.0 (GraphPad Software, CA, USA) is used to fit the data.

3. Results

3.1. Guinier plots of native TF variants at different concentrations

Fig. 1 shows Guinier plots of TF variants at various concentrations. The protein data should be fitted to a straight line on the Guinier plot; if they cannot be fitted to a straight line, but rather a polyline, this indicates protein aggregation [30]. No aggregation was observed for TF; MC shows some aggregation; and obvious aggregation was observed for TF419 and TF360. This indicates that the C-domain plays a critical role in the structural stability of TF.

The square of the apparent radius of gyration $R_g(c)$ and I(0) at various protein concentrations is estimated by Guinior approximation, the plot of $R_g(c)$ against c is shown in Fig. 2A, and fitted by the following equation:

$$R_g(c)^2 = R_g(0)^2 - B_{if}c \tag{10}$$

$R_g(0)$, the radius of gyration at infinite dilution, is calculated by the intercept of the equation and B_{if}, which is the parameter reflecting the intersolute force potential, is calculated by the slope of the equation [44,45].

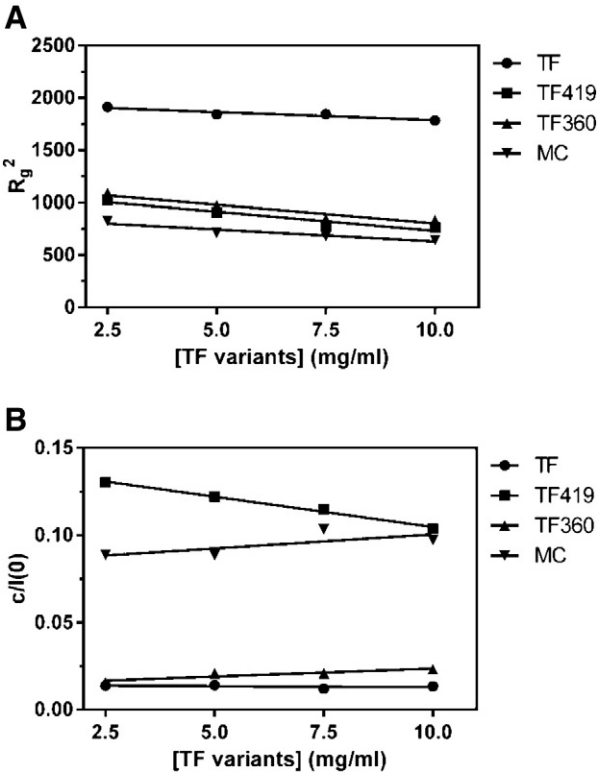

Fig. 2. Protein concentration dependence of $R_g(c)$ (A) and c/I(0) (B). The values of $R_g(c)$ and c/I(0) were calculated as described in Section 2.

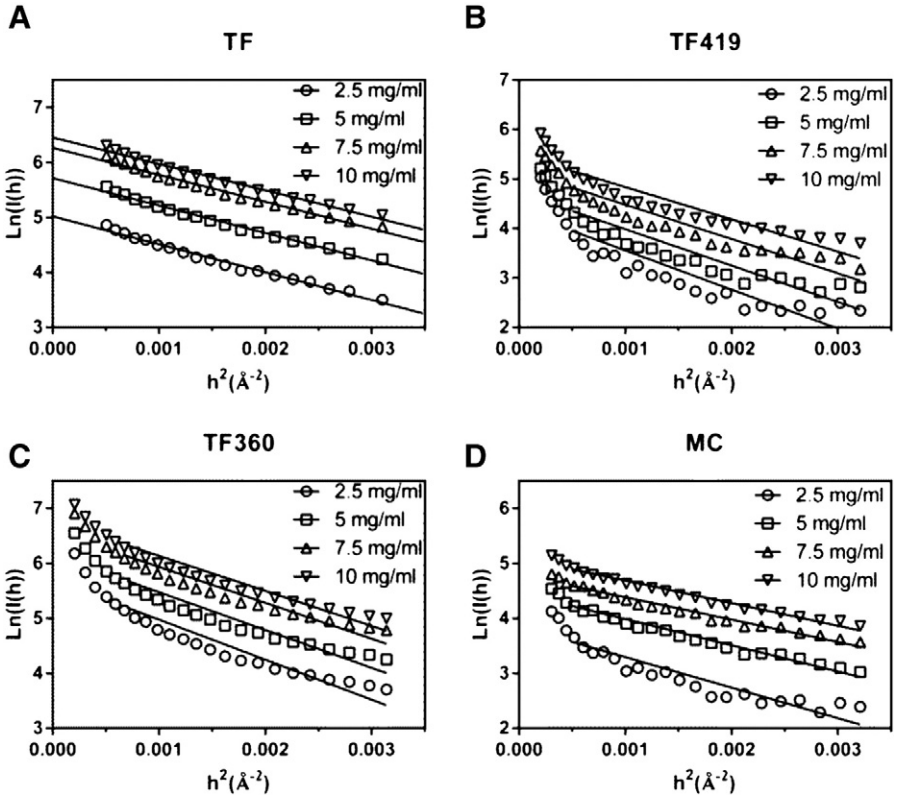

Fig. 1. Dependence of Guinier plots on TF (A), TF419 (B), TF360 (C) and MC (D) concentrations. The protein concentrations were 2.5, 5, 7.5 and 10 mg/ml, respectively. The straight lines were fitted with determined data in a range of 0.0005–0.0035 Å^{-2} using the least squares method.

Table 1
Structural parameters of TF variants determined with SAXS experiments. $R_g(0)$ is the radius of gyration at infinite dilution, A_2 is the second virial constant and B_{if} is a parameter reflecting the intersolute force potential. The data are presented as values ± standard deviations.

TF variants	$R_g(0)$ (Å)	A_2 (10^{-4} ml mol g^{-2})	B_{if} (10^{-13} cm^3 g^{-1})
TF	44.07 ± 0.3	−1.2 ± 1.8	−15.41 ± 3.86
TF419	33.09 ± 0.8	−37 ± 5	−36.37 ± 7.86
TF360	34.03 ± 0.74	9.16 ± 2.67	−35.52 ± 7.48
MC	29.28 ± 0.61	16.17 ± 10.87	−22.69 ± 5.29

I(0) is proportional to the molecular weight of the scatterer, the quantity that is proportional to c is $c/I(0)$ rather than $I(0)/c$ as

$$Kc/I(0) = 1/M + 2A_2c \quad (11)$$

where M is the molecular weight of the protein, K is a constant, and A_2 is the second virial constant [44–46]. The plot of $c/I(0)$ against c is shown in Fig. 2B, the A_2 values are estimated by the slope of the equation.

Table 1 lists the SAXS parameters. $R_g(0)$ are calculated to be 44.07 ± 0.3, 33.09 ± 0.8, 34.03 ± 0.74, 29.28 ± 0.61 Å for TF, TF419, TF360 and MC, respectively. The $R_g(0)$ value of TF is 33.18% bigger than TF419, which may be due to different dimerization ability of TF and TF419 [37,47]. The $R_g(0)$ value of TF360 is a little bigger than TF419, indicating that TF360 may undergo a more relaxed conformation than TF419. The $R_g(0)$ value of MC suggests that MC has a globular conformation. B_{if} is negative for all TF variants. The negative values of TF419, TF360 and MC are larger than that of TF, indicating stronger attractive interactions between TF419, TF360 and MC molecules. A_2, which is an indication of inter-particle interference effect [46], is negative for TF and TF419 and positive for TF360 and MC.

3.2. Kratky plot during urea-induced unfolding

Expressing the intensity function in the form of a Kratky plot has been shown to be useful for protein-folding studies and has been applied to the description of protein denaturation [46]. Information about molecular globularity can be obtained from the entire scattering pattern by plotting $I(h)h^2$ against h [46,48]. It is known that the presence of a peak in a Kratky plot indicates a native globular shape of a molecule, while a plateau in moderate angles of the plot indicates a chain-like structure [46,48]. Thus, it is easy to distinguish the shape of various conformational states [46,48]. Fig. 3 shows the Kratky plots of proteins in the range of 0–6 M urea. TF exhibits a clear peak in the absence of urea, indicating that native TF has a compact conformation. For urea of 0.5 and 1 M, the curve of TF is similar to that of TF in its native state; at 1.5 M, the curve has no peaks and exhibits a plateau, indicating that the TF is unfolding; at 3 M urea, the TF is completely unfolded. MC also exhibits a peak but it is not as clear as that of TF, indicating that the conformation of MC is looser than that of TF. At 0.5 M urea, the curve of MC is similar to that in its native state; at 1 and 1.5 M urea, the shape of plot differs from that in the native state, indicating a different conformation; at 2 M, MC is unfolded. TF419 has no clear peak in its native state, indicating that it does not have a compact structure; at 2 M urea, TF419 is unfolded. TF360 has no clear peak in its native state and is unstable. It is unfolded at urea concentrations as low as 0.5 M.

The peak intensities decreased gradually with increasing urea concentrations [49]. Fig. 4 shows the peak intensities during the urea-induced unfolding transition of TF variants. All exhibited a single sigmoidal transition and obeyed the two-state unfolding model. The thermodynamic parameters of the standard Gibbs free energies (ΔG^0), which represent the difference between the free energy of the folded and the unfolded states of the protein, and the slopes of the free energies versus denaturant concentrations (m_G), which indicate the change in the solvent-accessible surface area (ASA) upon unfolding, were obtained through data fitting, using Eqs. (1)–(6); The C_m values, which represent the denaturant concentration at which 50% of the molecules are folded, were also calculated according to Eq. (6) after setting $\Delta G = 0$. Table 2 gives the results. The ΔG^0 values for TF, TF419, TF360 and MC are 8.21 ± 1.48, 2.33 ± 0.44, 1.55 ± 0.32, 2.93 ± 1.02 KJ·mol^{-1}, respectively, indicating that the stability of TF decreases dramatically while C-terminal 13- and 72-residue was deleted and the

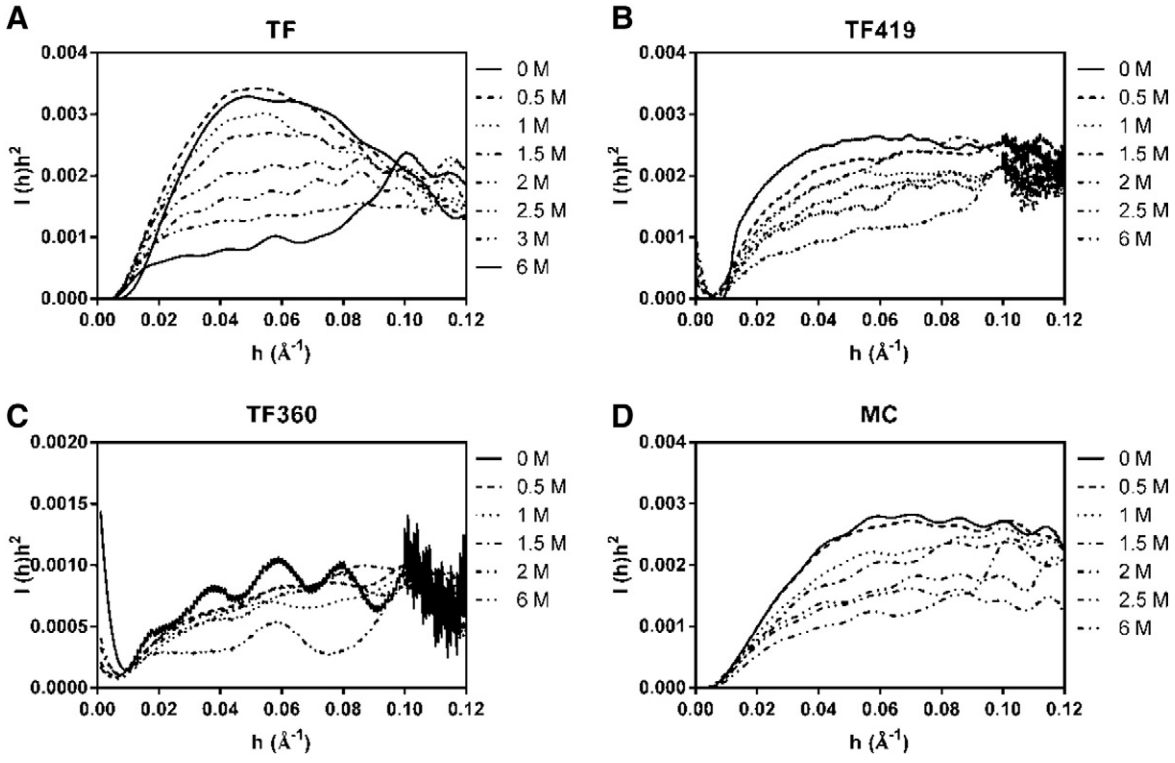

Fig. 3. Kratky plots of TF (A), TF419 (B), TF360 (C) and MC (D) in various concentrations of urea. The concentration of TF variants is 5 mg/ml.

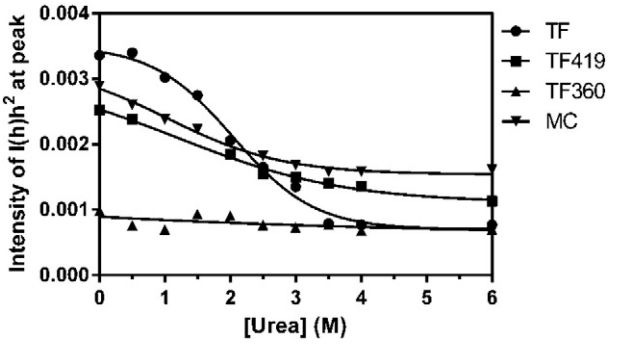

Fig. 4. Urea-induced equilibrium unfolding transitions for TF, TF419, TF360 and MC derived from I(h)h^2 intensity at the peaks. Data were fitted to a native-unfolding, two-state model (see Section 2).

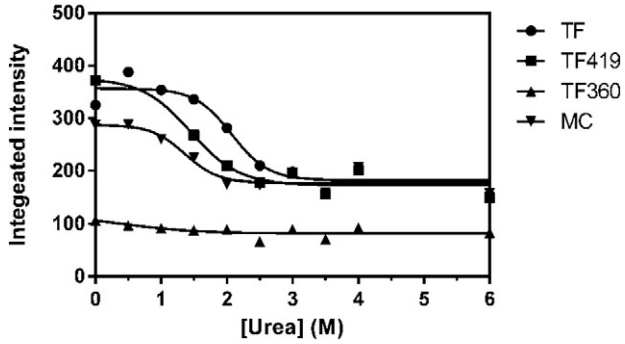

Fig. 5. Urea-induced equilibrium unfolding transitions for TF, TF419, TF360 and MC derived from integrated intensity. Data were fitted to a native-unfolding two state model (see Section 2).

stability of TF also decreases while N-domain was deleted. The C_m values for TF, TF419, TF360 and MC are 2.05 ± 0.11, 1.2 ± 0.31, 0.37 ± 0.21, 1.04 ± 0.34 M, respectively, also show the stability changes of TF variants as the ΔG^0 values show. The m_G values, for TF, TF419, TF360 and MC are 4.01 ± 0.64, 1.94 ± 0.69, 1.38 ± 0.56, 2.81 ± 0.63 KJ·mol^{-1}·M^{-1}, respectively.

3.3. Integrated intensity during urea-induced unfolding

In the globular state, the small-angle integrated intensity of a protein is large but it decreases as the protein changes to a coiled state [38]. The small-angle integrated intensity provides a good indication of the globular-to-coil transition, as it is much less sensitive to intermolecular association than the zero-angle intensity and the radius of gyration of a protein [38]. The integrated intensities within the region of h from 0.015 to 0.15 Å^{-1} during the urea-induced unfolding transition of TF variants are shown in Fig. 5; the data are fitted to a two-state unfolding model; ΔG^0, m_G and C_m values were obtained through the data fitting, using Eqs. (3)–(9). The results are shown in Table 2. The ΔG^0 values for TF, TF419, TF360 and MC are 18.43 ± 10.16, 9.8 ± 7.01, 1.68 ± 0.65, 13.3 ± 9.48 KJ·mol^{-1}, respectively; the C_m values for TF, TF419, TF360 and MC are 2.07 ± 0.17, 1.45 ± 0.22, 0.39 ± 0.33, 1.36 ± 0.19 M, respectively; the m_G values for TF, TF419, TF360 and MC are 8.89 ± 4.85, 6.77 ± 4.21, 4.31 ± 3.38, 9.78 ± 6.47 KJ·mol^{-1}·M^{-1}, respectively.

3.4. The changes in the R_g and I(0) values during urea-induced unfolding

The R_g and I(0) values of TF variants during urea-induced unfolding are calculated by Debye function and shown in Fig. 6. The R_g values of TF variants become bigger with the increase of urea concentration, indicating the transition from the native globular state to completely unfolded state such as random coils. The changes of R_g values during the urea-induced unfolding transition of TF variants are similar to the changes monitored by Kratky plot and integrated intensity.

I(0) is proportional to molecular weight and sensitive to association/disassociation during unfolding [46]. The I(0) values increase with the increase of urea concentration at low urea concentration (<3 M urea) which suggests aggregation within the unfolding transition region, and then decrease with urea concentration at high urea concentration (>3 M urea) which suggests that the aggregation is dispersed at higher urea concentrations.

3.5. P(r) function

The distance-distribution function, $P(r)$, can be obtained from the Fourier transform of the intensity function. Since $P(r)$ is an expression of the scattering curve in real space it is useful for intuitive interpretation of the conformation [33]. A unimodal $P(r)$ function is characteristic of a globular protein [33]. The largest dimension of the scatterer, D_{max}, is estimated from the point where the function approaches zero. Some proteins show aggregation, so the two-exponential equation $I = I(0)_1\exp(-(R_{g1}^2h^2/3)) + I(0)_2\exp(-(R_{g2}^2h^2/3))$ was used to subtract the intensity of aggregation and obtain the $P(r)$ function of the native proteins [30]. Fig. 7 shows the $P(r)$ function of proteins in their native and unfolding states. The $P(r)$ function of TF in solution shows a unimodal peak at 35.8 Å and D_{max} at 120 Å, indicating that TF has a compact global conformation in solution. The $P(r)$ function of MC shows a unimodal peak at 28.8 Å, coincident with R_g calculated from Kratky and Guinier plots. The D_{max} of MC is about 180 Å. This indicates that MC has a compact conformation but experiences some aggregation in solution. The $P(r)$ functions of TF419 and TF360 have a wide distribution, possibly due to severe aggregation. Even after removing the aggregation, TF360 exhibits a bimodal $P(r)$ function that is arguably a common structural property in partially-unfolded conformations [46], or where there are two centers of mass. Thus, TF360 may have partially-unfolded conformations in its native state, or two centers of mass, such as in a dumbbell shape.

4. Discussion

Here we used SAXS to study the effect of the N- and C-domains on TF stability; a Guinier plot showed that full-length TF exhibits no aggregation at all the concentrations (2.5, 5, 7.5 and 10 mg/ml) we tested

Table 2
Thermodynamic parameters for urea denaturation of TF variants. ΔG^0 is the standard Gibbs free energies upon unfolding in the absence of denaturants, m_G is the slopes of the free energies versus denaturant concentrations, and C_m is the denaturant mid-point of the transition. The data are presented as values ± standard deviations.

Protein	Intensity of I(h)h^2 at peak			Integrated intensity		
	ΔG^0 (KJ·mol^{-1})	m_G (KJ·mol^{-1}·M^{-1})	C_m (M)	ΔG^0 (KJ·mol^{-1})	m_G (KJ·mol^{-1}·M^{-1})	C_m (M)
TF	8.21 ± 1.48	4.01 ± 0.64	2.05 ± 0.11	18.43 ± 10.16	8.89 ± 4.85	2.07 ± 0.17
TF419	2.33 ± 0.44	1.94 ± 0.69	1.2 ± 0.31	9.8 ± 7.01	6.77 ± 4.21	1.45 ± 0.22
TF360	1.55 ± 0.32	1.38 ± 0.56	0.37 ± 0.21	1.68 ± 0.65	4.31 ± 3.38	0.39 ± 0.33
MC	2.93 ± 1.02	2.81 ± 0.63	1.04 ± 0.34	13.3 ± 9.48	9.78 ± 6.47	1.36 ± 0.19

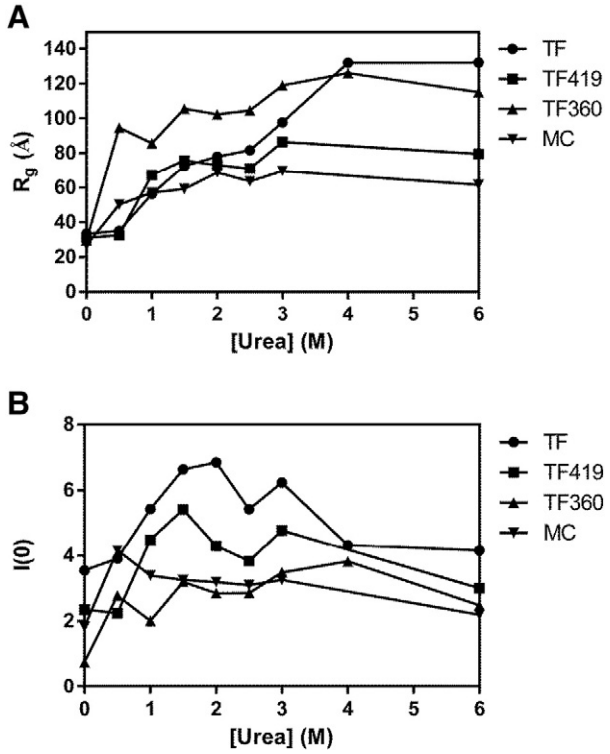

Fig. 6. Urea-induced equilibrium unfolding transitions for TF, TF419, TF360 and MC derived from R_g and I(0) values, estimated using the Guinier or Debye approximations (see Section 2).

(Fig. 1). TF419 and TF360 exhibited severe aggregation and MC had little aggregation (Fig. 1). B_{if} values of TF variants which indicate the attractive interactions between the molecules suggested the same inference (Table 1).

We tested the stability of TF variants in various concentrations of urea; the Kratky plots are shown in Fig. 3. We analyzed the urea-induced transition of TF variants, fitting the data to a native-unfolding, two-state model (Figs. 4 and 5). Table 2 gives the parameters. The changes in the R_g and I(0) values during urea-induced unfolding are shown in Fig. 6. These results indicate that structural stability decreases with the length of the C-terminal truncation; TF stability decreased significantly with truncation of C-terminal 13-residue and almost lost its structure entirely and unfolded when C-terminal 72-residue truncated. MC, however, maintained a compact structure. Its stability decreased when the entire N-domain was truncated, suggesting that the N-domain interacts with the M- and C-domains, but the interaction is weak.

The $P(r)$ function (Fig. 7) demonstrated that full length TF has nearly the same structure in crystal and in solution; TF419 exhibits some aggregation, TF360 has significant aggregation and moves to a partly unfolded state, suggesting that C-terminal 72-residue is necessary for maintaining the structural stability of the molecule. MC shows aggregation but maintains a compact conformation, indicating that the N-domain helps stabilize the intact molecule, but the effect is weak.

The crystal structure of *E. coli* TF shows an interesting arrangement of domains that has been likened to the image of a crouching dragon. The N-domain is its tail and the C-domain (arms) are brought together, while the middle PPIase domain protrudes from the structure, forming the dragon's head. In the ribosome-bound form, the dragon is anchored by its N-domain tail and hunches over the exit of the ribosome tunnel, providing a protected folding environment or cradle for emerging nascent peptides. The inner surface of the cradle presents a hydrophobic surface to the nascent peptide that is formed by residues from the N- and C-domains [23]. Biochemical data show that only the isolated C-domain or combinations with C (NC, MC) provide substantial chaperone activity in vitro and in vivo. Domain combinations without the C-domain (NM) showed little chaperone activity in vitro or in vivo [50]. The deletion of the C-terminal 13 amino acid residues caused a dramatic difference in the extent and mode of TF-assisted GAPDH refolding, whereas the

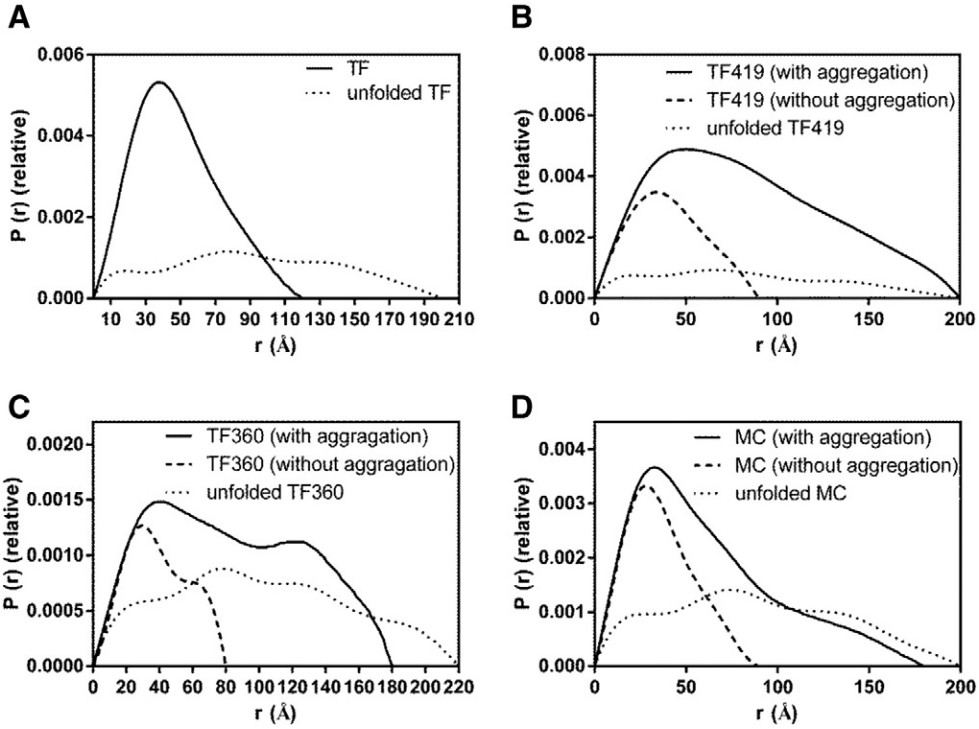

Fig. 7. $P(r)$ function of TF, TF419, TF360 and MC. The $P(r)$ values of TF, TF419, TF360 and MC were calculated from the experimental scattering curves using the GNOM program. The solid lines are P(r) of TF variants in solution, the dash lines are P(r) of TF variants without aggregation in solution which is achieved by subtracting the scattering of aggregation from the TF variants in solution (see Section 3), the dot lines are P(r) of unfolded TF variants in 6 M urea.

deletion of C-terminal 72 amino acid residues made no difference [37]. The deletion of the C-terminal 53 amino acid residues completely eliminated the chaperone activity of TF in vitro and severely impaired its function in vivo [20]. These results agree with our results.

5. Conclusion

C-terminal 72-residue is necessary for maintaining the structural stability of the molecule while the N-domain helps stabilize the intact molecule but has less influence on its structural stability.

Abbreviations

SAXS, small-angle X-ray scattering; TF, trigger factor

Acknowledgment

SAXS measurements were performed under proposal number 2004G386 of the Photon Factory.

References

[1] W.A. Houry, Chaperone-assisted protein folding in the cell cytoplasm, Curr. Protein Pept. Sci. 2 (2001) 227–244.
[2] F.U. Hartl, M. Hayer-Hartl, Molecular chaperones in the cytosol: from nascent chain to folded protein, Science 295 (2002) 1852–1858.
[3] E. Deuerling, B. Bukau, Chaperone-assisted folding of newly synthesized proteins in the cytosol, Crit. Rev. Biochem. Mol. Biol. 39 (2004) 261–277.
[4] J.C. Young, V.R. Agashe, K. Siegers, F.U. Hartl, Pathways of chaperone-mediated protein folding in the cytosol, Nat. Rev. Mol. Cell Biol. 5 (2004) 781–791.
[5] V.R. Agashe, S. Guha, H.C. Chang, P. Genevaux, M. Hayer-Hartl, M. Stemp, C. Georgopoulos, F.U. Hartl, J.M. Barral, Function of trigger factor and DnaK in multidomain protein folding: increase in yield at the expense of folding speed, Cell 117 (2004) 199–209.
[6] R.S. Ullers, E.N. Houben, A. Raine, C.M. ten Hagen-Jongman, M. Ehrenberg, J. Brunner, B. Oudega, N. Harms, J. Luirink, Interplay of signal recognition particle and trigger factor at L23 near the nascent chain exit site on the *Escherichia coli* ribosome, J. Cell Biol. 161 (2003) 679–684.
[7] R. Maier, B. Eckert, C. Scholz, H. Lilie, F.X. Schmid, Interaction of trigger factor with the ribosome, J. Mol. Biol. 326 (2003) 585–592.
[8] E. Deuerling, H. Patzelt, S. Vorderwulbecke, T. Rauch, G. Kramer, E. Schaffitzel, A. Mogk, A. Schulze-Specking, H. Langen, B. Bukau, Trigger factor and DnaK possess overlapping substrate pools and binding specificities, Mol. Microbiol. 47 (2003) 1317–1328.
[9] G.C. Huang, J.J. Chen, C.P. Liu, J.M. Zhou, Chaperone and antichaperone activities of trigger factor, Eur. J. Biochem. 269 (2002) 4516–4523.
[10] E. Schaffitzel, S. Rudiger, B. Bukau, E. Deuerling, Functional dissection of trigger factor and DnaK: interactions with nascent polypeptides and thermally denatured proteins, Biol. Chem. 382 (2001) 1235–1243.
[11] R. Maier, C. Scholz, F.X. Schmid, Dynamic association of trigger factor with protein substrates, J. Mol. Biol. 314 (2001) 1181–1190.
[12] G.C. Huang, Z.Y. Li, J.M. Zhou, G. Fischer, Assisted folding of D-glyceraldehyde-3-phosphate dehydrogenase by trigger factor, Protein Sci. 9 (2000) 1254–1261.
[13] S.A. Teter, W.A. Houry, D. Ang, T. Tradler, D. Rockabrand, G. Fischer, P. Blum, C. Georgopoulos, F.U. Hartl, Polypeptide flux through bacterial Hsp70: DnaK cooperates with trigger factor in chaperoning nascent chains, Cell 97 (1999) 755–765.
[14] E. Deuerling, A. Schulze-Specking, T. Tomoyasu, A. Mogk, B. Bukau, Trigger factor and DnaK cooperate in folding of newly synthesized proteins, Nature 400 (1999) 693–696.
[15] C. Scholz, G. Stoller, T. Zarnt, G. Fischer, F.X. Schmid, Cooperation of enzymatic and chaperone functions of trigger factor in the catalysis of protein folding, EMBO J. 16 (1997) 54–58.
[16] O. Kandror, M. Sherman, R. Moerschell, A.L. Goldberg, Trigger factor associates with GroEL in vivo and promotes its binding to certain polypeptides, J. Biol. Chem. 272 (1997) 1730–1734.
[17] O. Kandror, A.L. Goldberg, Trigger factor is induced upon cold shock and enhances viability of *Escherichia coli* at low temperatures, Proc. Natl. Acad. Sci. U. S. A. 94 (1997) 4978–4981.
[18] T. Hesterkamp, E. Deuerling, B. Bukau, The amino-terminal 118 amino acids of *Escherichia coli* trigger factor constitute a domain that is necessary and sufficient for binding to ribosomes, J. Biol. Chem. 272 (1997) 21865–21871.
[19] C.P. Liu, Q.M. Zhou, D.J. Fan, J.M. Zhou, PPIase domain of trigger factor acts as auxiliary chaperone site to assist the folding of protein substrates bound to the crevice of trigger factor, Int. J. Biochem. Cell Biol. 42 (2010) 890–901.
[20] F. Merz, A. Hoffmann, A. Rutkowska, B. Zachmann-Brand, B. Bukau, E. Deuerling, The C-terminal domain of *Escherichia coli* trigger factor represents the central module of its chaperone activity, J. Biol. Chem. 281 (2006) 31963–31971.
[21] Y. Shi, D.J. Fan, S.X. Li, H.J. Zhang, S. Perrett, J.M. Zhou, Identification of a potential hydrophobic peptide binding site in the C-terminal arm of trigger factor, Protein Sci. 16 (2007) 1165–1175.
[22] O. Kristensen, M. Gajhede, Chaperone binding at the ribosomal exit tunnel, Structure 11 (2003) 1547–1556.
[23] L. Ferbitz, T. Maier, H. Patzelt, B. Bukau, E. Deuerling, N. Ban, Trigger factor in complex with the ribosome forms a molecular cradle for nascent proteins, Nature 431 (2004) 590–596.
[24] A.V. Ludlam, B.A. Moore, Z. Xu, The crystal structure of ribosomal chaperone trigger factor from *Vibrio cholerae*, Proc. Natl. Acad. Sci. U. S. A. 101 (2004) 13436–13441.
[25] D. Baram, E. Pyetan, A. Sittner, T. Auerbach-Nevo, A. Bashan, A. Yonath, Structure of trigger factor binding domain in biologically homologous complex with eubacterial ribosome reveals its chaperone action, Proc. Natl. Acad. Sci. U. S. A. 102 (2005) 12017–12022.
[26] F. Schlunzen, D.N. Wilson, P. Tian, J.M. Harms, S.J. McInnes, H.A. Hansen, R. Albrecht, J. Buerger, S.M. Wilbanks, P. Fucini, The binding mode of the trigger factor on the ribosome: implications for protein folding and SRP interaction, Structure 13 (2005) 1685–1694.
[27] M. Vogtherr, D.M. Jacobs, T.N. Parac, M. Maurer, A. Pahl, K. Saxena, H. Ruterjans, C. Griesinger, K.M. Fiebig, NMR solution structure and dynamics of the peptidyl-prolyl cis-trans isomerase domain of the trigger factor from *Mycoplasma genitalium* compared to FK506-binding protein, J. Mol. Biol. 318 (2002) 1097–1115.
[28] E. Martinez-Hackert, W.A. Hendrickson, Structures of and interactions between domains of trigger factor from *Thermotoga maritima*, Acta Crystallogr. D Biol. Crystallogr. 63 (2007) 536–547.
[29] E. Martinez-Hackert, W.A. Hendrickson, Promiscuous substrate recognition in folding and assembly activities of the trigger factor chaperone, Cell 138 (2009) 923–934.
[30] G. Porod, Small Angle X-ray Scattering, Academic Press, London, 1982.
[31] A. Guinier, G. Fournet, Small Angle Scattering X-rays, John Wiley & Sons, New York, 1955.
[32] D.I. Svergun, Restoring low resolution structure of biological macromolecules from solution scattering using simulated annealing, Biophys. J. 76 (1999) 2879–2886.
[33] T. Konno, M. Kataoka, Y. Kamatari, K. Kanaori, A. Nosaka, K. Akasaka, Solution X-ray scattering analysis of cold- heat-, and urea-denatured states in a protein, *Streptomyces subtilisin* inhibitor, J. Mol. Biol. 251 (1995) 95–103.
[34] L. Zhu, H. Kihara, M. Kojima, J.M. Zhou, S. Perrett, Small angle X-ray scattering study of the yeast prion Ure2p, Biochem. Biophys. Res. Commun. 311 (2003) 525–532.
[35] J.M. Zhou, Y.X. Fan, H. Kihara, K. Kimura, Y. Amemiya, The compactness of ribonuclease A and reduced ribonuclease A, FEBS Lett. 430 (1998) 275–277.
[36] J.M. Zhou, Y.X. Fan, H. Kihara, K. Kimura, Y. Amemiya, Unfolding of dimeric creatine kinase in urea and guanidine hydrochloride as measured using small angle X-ray scattering with synchrotron radiation, FEBS Lett. 415 (1997) 183–185.
[37] L.L. Zeng, L. Yu, Z.Y. Li, S. Perrett, J.M. Zhou, Effect of C-terminal truncation on the molecular chaperone function and dimerization of *Escherichia coli* trigger factor, Biochimie 88 (2006) 613–619.
[38] G.V. Semisotnov, H. Kihara, N.V. Kotova, K. Kimura, Y. Amemiya, K. Wakabayashi, I.N. Serdyuk, A.A. Timchenko, K. Chiba, K. Nikaido, T. Ikura, K. Kuwajima, Protein globularization during folding. A study by synchrotron small-angle X-ray scattering, J. Mol. Biol. 262 (1996) 559–574.
[39] I. Pilz, O. Glatter, O. Kratky, Small-angle X-ray scattering, Methods Enzymol. 61 (1979) 148–249.
[40] M. Kataoka, Y. Hagihara, K. Mihara, Y. Goto, Molten globule of cytochrome c studied by small angle X-ray scattering, J. Mol. Biol. 229 (1993) 591–596.
[41] D.I. Svergun, Determination of the regularization parameter in indirect-transform methods using perceptual criteria, J. Appl. Crystallogr. 25 (1992) 495–503.
[42] C.R. Cantor, P.R. Schimmel, Biophysical Chemistry, W.H. Freeman and Company, San Francisco, CA, 1980.
[43] Y. Shi, D. Zheng, J. Xie, Q. Zhang, H. Zhang, Thermal stability of *Thermoanaerobacter tengcongensis* ribosome recycling factor, Protein Pept. Lett. 21 (2014) 285–291.
[44] Y.Y. Shi, X.G. Hong, C.C. Wang, The C-terminal (331–376) sequence of *Escherichia coli* DnaJ is essential for dimerization and chaperone activity: a small angle X-ray scattering study in solution, J. Biol. Chem. 280 (2005) 22761–22768.
[45] S.J. Li, X.G. Hong, Y.Y. Shi, H. Li, C.C. Wang, Annular arrangement and collaborative actions of four domains of protein–disulfide isomerase: a small angle X-ray scattering study in solution, J. Biol. Chem. 281 (2006) 6581–6588.
[46] M. Kataoka, I. Nishii, T. Fujisawa, T. Ueki, F. Tokunaga, Y. Goto, Structural characterization of the molten globule and native states of apomyoglobin by solution X-ray scattering, J. Mol. Biol. 249 (1995) 215–228.
[47] Y. Shi, L. Yu, H. Kihara, J.M. Zhou, C-terminal 13-residue truncation induces compact trigger factor conformation and severely impairs its dimerization ability, Protein Pept. Lett. 21 (2014) 476–482.
[48] M. Kojima, M. Tanokura, M. Maeda, K. Kimura, Y. Amemiya, H. Kihara, K. Takahashi, pH-dependent unfolding of aspergillopepsin II studied by small-angle X-ray scattering, Biochemistry 39 (2000) 1364–1372.
[49] T. Higurashi, Y. Hiragi, K. Ichimura, Y. Seki, K. Soda, T. Mizobata, Y. Kawata, Structural stability and solution structure of chaperonin GroES heptamer studied by synchrotron small-angle X-ray scattering, J. Mol. Biol. 333 (2003) 605–620.
[50] G. Kramer, A. Rutkowska, R.D. Wegrzyn, H. Patzelt, T.A. Kurz, F. Merz, T. Rauch, S. Vorderwulbecke, E. Deuerling, B. Bukau, Functional dissection of *Escherichia coli* trigger factor: unraveling the function of individual domains, J. Bacteriol. 186 (2004) 3777–3784.